Fiber-Rotation-Induced Vortex Turbulence in Thick Myocardium

Flavio Fenton and Alain Karma

Department of Physics and Center for Interdisciplinary Research on Complex Systems, Northeastern University, Boston, Massachusetts 02115

(Received 25 February 1998)

The ventricle is a strongly anisotropic three-dimensional excitable medium. Waves of electrical activity propagate faster parallel to the long axis of the muscle fibers. Moreover, this axis rotates intramurally across the ventricular wall. It is demonstrated that this rotating anisotropy can cause a transmural scroll vortex filament to spontaneously decay into wave turbulence above a minimum wall thickness comparable to the one necessary to sustain ventricular fibrillation. Moreover, the instability that produces this decay is shown to be associated with the propagation of localized twist-induced disturbances along the filament. [S0031-9007(98)06591-0]

PACS numbers: 87.22.Jb, 47.27.–i, 47.54.+r

Over the last decade spiral and scroll waves of electrical activity in cardiac tissue have become a major focus of research because of their central role in arrhythmogenesis [1]. They are life threatening because they act as high frequency sources of waves that can produce tachycardia, an abnormally rapid contraction rhythm no longer controlled by the heart's natural pacemaker. Once initiated in a healthy tissue, ventricular tachycardia (VT) usually decays in a few seconds into ventricular fibrillation (VF), a more spatiotemporally disorganized electrical activity that destroys the main pumping function of the muscle and leads to sudden cardiac death.

One central question [2], still actively debated [3], is whether the wave instability that causes VF is two or three dimensional in nature. A number of wall-thinning experiments [4–6] indicate that a minimum ventricular wall thickness is required to induce VF. In these experiments, a finite thickness of ventricular tissue is destroyed. VT is then induced electrically in the surviving thinner tissue by a premature stimulus. If the thickness of spared tissue is more than about 3–4 mm, VT decays into VF, while if it is less, VT is sustained.

By now, a number of simulations of various reaction-diffusion models have shown that both transient [7] and sustained [8] "VF-like" spiral wave turbulence can be induced in a 2D excitable medium by various wave breakup mechanisms. These mechanisms, however, do not as such explain the aforementioned results of the wall-thinning experiments where the three dimensionality of the tissue seems to play a crucial role. This paradoxical situation has recently led Winfree to hypothesize [2] that some vortex filament instability may be involved in VF, but the origin of such instability has so far remained unclear. Panfilov and Hogeweg have found that scroll breakup can occur in 3D [9], also by a plane wave instability mechanism, in a parameter range of a modified FitzHugh-Nagumo (FN) model where spiral breakup is absent in 2D. This parameter range, however, is extremely narrow and therefore unlikely to be germane to most experiments. Biktashev *et al.* have shown that vortex filaments can become unstable due to a negative filament tension [10]. The tension, however, is generally only negative for a weakly excitable tissue, close to the margin of propagation failure. While ischemic tissue (i.e., with a reduced blood supply) can become weakly excitable, normal myocardium is typically highly excitable. Finally, Panfilov and Keener [11] have shown that scroll breakup can occur in 3D due to fiber rotation. However, breakup in their model only occurred on a very coarse lattice with a spacing of about 1 mm between layers, and was suppressed by refining the mesh. Aside from macroscopic inhomogeneities, discrete effects are expected to be on a much finer scale of the cell size ($\sim 100\ \mu$m). Because the width of the excitation wave front (i.e., wave speed $\times$ rise time of excitation) is comparatively about 1 order of magnitude larger (~ 1 mm), wave propagation in myocardium has been traditionally modeled by continuum equations. Therefore, it remains uncertain to what extent instabilities tied to a coarse discretization are relevant.

In this Letter, we model myocardium as a continuous excitable medium with a rotating anisotropy. We show that this anisotropy can destabilize vortex filaments and produce a transition to wave turbulence characteristic of VF above a minimum wall thickness and fiber rotation rate. We pinpoint the nature of this instability by examining the spatiotemporal dynamics of twist along the filament. We find that it differs from the twist-induced helical instability of scroll filaments in an isotropic medium (sproing) [12], where the twist is uniformly distributed along the filament. In contrast, here, twist is concentrated in pulselike entities, referred to hereafter as twistons, which propagate along the filament and produce a complex spatiotemporal vortex dynamics. We simulate the standard continuous cable equations

$$\partial_t V = \partial_{x_i}(D_{ij}\partial_{x_j} V) - I_{\rm ion}/C_m\,, \qquad (1)$$

in an idealized parallelepipedal slab of ventricular tissue of wall thickness, L, parametrized by the Cartesian

coordinates (x_1, x_2, x_3) where we have assumed summation over the repeated indices i and j. V is the transmembrane potential in mV, $I_{\rm ion}$ is the total ionic current flowing through the membrane in μA/cm^2, C_m is the membrane capacitance set equal to 1 μF/cm^2, and time is in units of msec. The muscle fibers are assumed to be parallel in each x_1-x_2 sheet. Furthermore, the angle between the fiber axis and the x_1 axis in each sheet, defined by $\theta(x_3) = -\Delta\theta/2 + x_3\,(\Delta\theta/L)$, is assumed to rotate continuously between the two surfaces of the slab ($x_3 = 0$ and $x_3 = L$) by a total angle $\Delta\theta$. The nonzero elements of the anisotropic diffusion tensor are given accordingly by $D_{11} = D_\parallel\,{\rm cs}^2 + D_{\perp 1}\,{\rm sn}^2$, $D_{22} = D_\parallel\,{\rm sn}^2 + D_{\perp 1}\,{\rm cs}^2$, $D_{12} = D_{21} = (D_\parallel - D_{\perp 1}){\rm cs\,sn}$, $D_{33} = D_{\perp 2}$, where ${\rm cs} \equiv \cos\theta(x_3)$ and ${\rm sn} \equiv \sin\theta(x_3)$. The diffusion constants corresponding to in-plane propagation parallel and perpendicular to the fiber, and transmurally, are chosen as $D_\parallel = 1$ cm^2/sec, $D_{\perp 1} = 0.2$ cm^2/sec, and $D_{\perp 2} = 0.2$ cm^2/sec, respectively. We consider the slab to be electrically insulated and impose accordingly that $n_i D_{ij} \partial_{x_j} V = 0$ on each face of the slab where $n_i = \pm\hat{x}_i$ ($i = 1, 2, 3$) is the normal to each face.

We base our study on a simplified three-variable (3V) ionic model of ventricular action potential developed in Ref. [13]. This model reproduces relatively faithfully the one-dimensional pulse dynamics and complex spiral wave behavior of higher order ionic models while remaining computationaly tractable in 3D. The parameters of this model are chosen here to mimic the membrane dynamics of the Beeler-Reuter model [14], modified to have a faster calcium kinetics (and referred to as MBR in [13]). This calcium speedup was introduced previously by Courtemanche and Winfree [7] and shown to suppress spiral wave breakup present in the original Beeler-Reuter equations. The membrane current, $I_{\rm ion}$, of the 3V model, is written as the sum, $I_{\rm ion} = I_{\rm fi} + I_{\rm so} + I_{\rm si}$, of a fast inward (Na) current, $I_{\rm fi}$, a slow outward (K) current, $I_{\rm so}$, and a slow inward (Ca) current, $I_{\rm si}$, defined by

$$I_{\rm fi}(V;h) = -0.04\,h(15 - V)(V + 72)p\,, \qquad (2)$$

$$I_{\rm so}(V) = (V + 85)(1 - p)/8.3 + 2p\,, \qquad (3)$$

$$I_{\rm si}(V;f) = -(1 + \tanh[0.1V])f/0.897\,, \qquad (4)$$

where h and f are gate variables that govern the activation and inactivation of $I_{\rm fi}$ and $I_{\rm si}$, respectively. Their kinetics are given by

$$\partial_t h = (1 - p)(1 - h)/[1000q + 19.2(1 - q)] - 0.3ph\,, \qquad (5)$$

$$\partial_t f = (1 - p)(1 - f)/11 - pf/667\,, \qquad (6)$$

where p and q are Heaviside step functions defined by $p = 1$ ($p = 0$) for $V \geq -72$ ($V < -72$), and $q = 1$ ($q = 0$) for $V \geq -79.5$ ($V < -79.5$).

We use as initial condition a transmural filament parallel to the x_3 axis obtained by stacking spiral waves obtained from an independent 2D simulation. The instantaneous filament position, defined here by $\mathbf{R}(s,t)$, where s is the arclength along the filament, is tracked intramurally by calculating the intersection line of the isopotential surface $V = -35$ mV and the surface $\partial_t V = 0$. We also calculate the twist

$$W(s,t) = [\partial_s \mathbf{N}(s,t) \times \mathbf{N}(s,t)] \cdot \mathbf{t}(s,t)\,, \qquad (7)$$

which measures the rate of angular rotation of the wave front per unit arclength s along the filament, where $\mathbf{N} = \nabla V/|\nabla V|$ is the unit vector locally perpendicular to the tangent to the filament defined by $\mathbf{t}(\mathbf{s},\mathbf{t}) \equiv \partial_s \mathbf{R}(s,t)/|\partial_s \mathbf{R}(s,t)|$. Finally, we use an efficient semi-implicit algorithm to time step Eqs. (1), (5), and (6), which is described in [13]. This allows us to use simultaneously a fine enough lattice spacing, here $\Delta x_i = 0.031$ cm ($i = 1, 2, 3$), to approach reasonably the continuum limit of the cable equations, and a large enough time step, $\Delta t = 0.25$ msec, to simulate a few seconds of reentry on a cubic lattice of dimension $200 \times 200 \times L/\Delta x_3$. Our results remain about 95% accurate with Δx twice smaller.

We vary L between 1 and 10 mm for several different fiber rotation rates, $F_r \equiv \Delta\theta/L = 0$, 6, 12, 20, and 30°/mm. The case of zero fiber rotation ($F_r = 0$) is equivalent to propagation in an isotropic medium after rescaling of the axis perpendicular to the fiber direction by a factor of $(D_{\perp 1}/D_\parallel)^{1/2}$. In this case, we find that, even if slightly perturbed, the filament relaxes to being parallel to the x_3 axis and untwisted. This is to be expected here because L is smaller than the spiral core size $\approx$2–3 cm. In contrast, with fiber rotation the filament becomes progressively more wiggly and twisted intramurally with increasing L. For $F_r = 6°$/mm, the dynamics remains dominated by the original transmural filament up to $L = 1$ cm. In contrast, for $F_r \geq 12°$/mm, there is a minimum wall thickness $L_{\rm min}$ above which the intramural wiggling (Fig. 1) becomes sufficient to cause a transition to a turbulent state characterized by a large average number of chaotically moving filaments (Fig. 2). This minimum is about 4–6 mm for a $F_r = 12°$/mm, which is roughly in agreement with the results of the left-ventricular wall-thinning experiments, and 3–4 mm for $F_r = 30°$/mm. Therefore we find that vortex turbulence requires both a minimum F_r in the range of 6–12°/mm, and a minimum wall thickness that only weakly decreases with increasing F_r. Since the total angle of fiber rotation is approximately constant, this minimum F_r implies that a ventricle with a sufficiently thick wall (2–3 cm and above) would not fibrillate by this instability.

The initial decay into turbulence is initiated by the intramural elongation and curving of the filament that makes it collide with either boundaries of the muscle (i.e., the epicardium or endocardium). A typical collision, which is illustrated in Fig. 1, cuts the original filament into two segments, one that remains transmural and the other corresponding to a half vortex ring attached to the

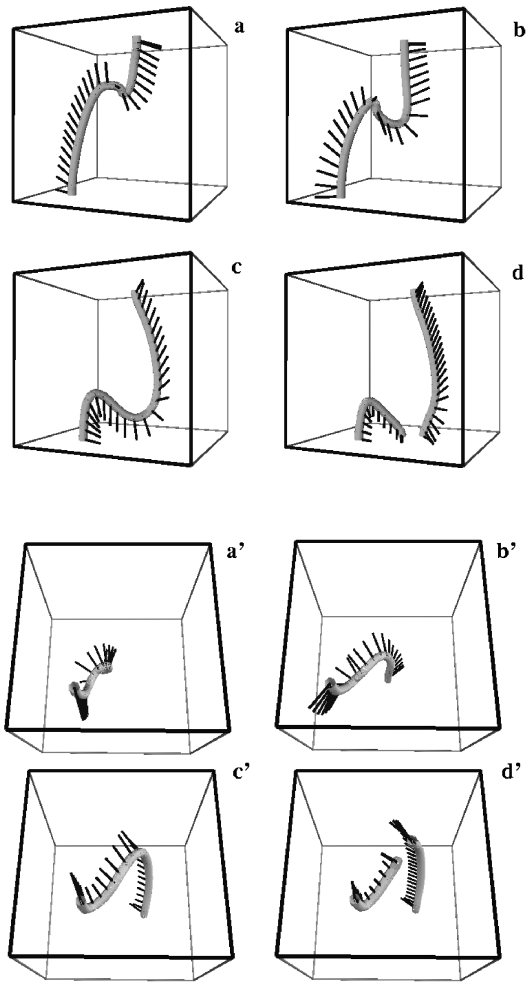

FIG. 1. Side (a)–(d) and bottom (a')–(d') perspectives of the filament shown at $t = 195$ [(a) and (a')], 207 [(b) and (b')], 220 [(c) and (c')], and 232 [(d) and (d')] msec for $L = 6.2$ mm and $F_r = 12°/\text{mm}$. For visualization, the scale of the x_3 axis is magnified 5 times and only part of the whole slab is represented.

colliding surface (bottom right frame of Fig. 1). This mechanism does not involve propagation failure, which has been commonly invoked to explain the formation of new vortices, but only topological changes of the filament. Subsequently, either the vortex ring contracts and only the transmural filament survives until another collision or it expands sufficiently to collide with the opposite boundary (top two frames of Fig. 2). In the latter case, two additional transmural filaments are formed by this collision in addition to the original one. Once several filaments are formed, the decay into turbulence is then further accelerated by additional processes. Vortex rings can spontaneously form intramurally, or attached to one boundary, by a traditional conduction block mechanism. In addition, separate filaments can join to form yet more complex configurations. Therefore, three dynamical regimes can be distinguished. First, for L smaller than $L_{\min}$, the filament becomes progressively more wiggly with increasing L, but the wiggles remain confined and

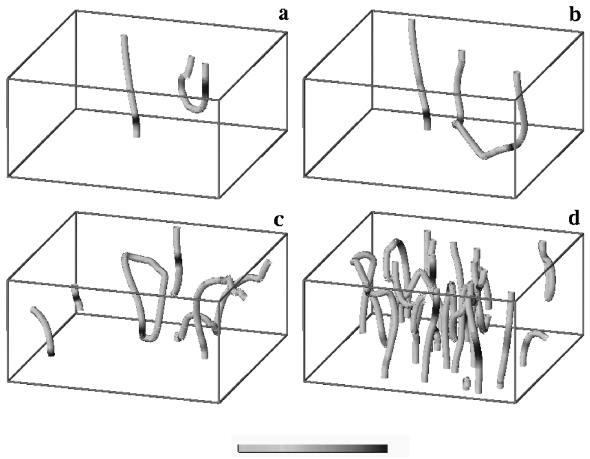

FIG. 2. Continuing sequence of Fig. 1 showing perspectives of the whole slab for $t = 410$ (a), 465 (b), 880 (c), and 1067 (d) msec. $|W(s,t)|$ is plotted along the filament with a grey scale ranging from light grey (zero twist) to black (50°/mm).

collisions do not occur. Second, in the weakly turbulent regime where L is comparable to $L_{\min}$, half rings are sporadically created by the collision process of Fig. 1 but they vanish systematically. Third, in the fully developed turbulence regime for L greater than $L_{\min}$ half vortex rings expand sufficiently frequently to produce additional transmural filaments. After that, the number of filaments increases during a transient of about 1 sec, and then fluctuates around some large average number.

Figures 1 and 3 illustrate the nature of the twist that produces the filament instability. In Fig. 1, twist is represented by plotting the vector $\mathbf{N} = \nabla V/|\nabla V|$ at equally spaced points along the filament. It can be seen that $\mathbf{N}$ changes orientation rapidly only along a short, and hence highly twisted, segment of the filament, which travels transmurally along the filament. The propagative nature of this instability is further illustrated in Fig. 3a where we plot stroboscopically the twist $W(s,t)$ vs the arclength s along the filament every 1.25 msec for about one average rotation period ($\approx$200 msec) of the scroll wave. The landscape of this space-time plot is composed for the most part of nearly flat valleys or gently rolling hills, of little twist activity, and abrupt oblique ridges that mark the transmural propagation of twistons. The slope of the ridges in this plot indicate that twistons propagate at a wave speed close to $c_{\perp 2}$, which is $\approx$20 cm/sec. Figure 3a shows that twistons are typically created just below one surface of the muscle (epicardium or endocardium) on average twice per period, and vanish at the opposite surface, thereby unwinding the filament on a time scale $\sim L/c_{\perp 2}$. It also reveals that the rise in twist amplitude that creates twistons takes place during the rapid pivot turn of the wave front around small outward petals of the complex meandering trajectory of the wave tip, on a time scale $t_{\text{piv}} \sim 10$–20 msec. This rise occurs because fiber rotation causes this pivot turn to take place asynchronously in the different fiber sheets

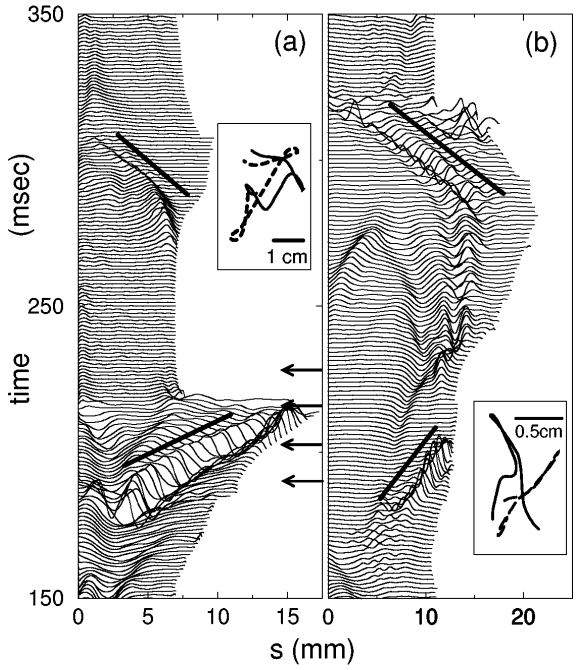

FIG. 3. Plot of twist vs arclength along the filament for (a) the reduced three-variable ionic model with $L = 6.2$ mm and $F_r = 12°/\text{mm}$, and (b) the standard FN model defined by $I_{\text{ion}}/C_m = (-3V + V^3 + g)$ and $\partial_t g = \epsilon(V - \delta)$, with $L = 1$ cm, $F_r = 12°/\text{mm}$, $\epsilon = 0.012$, $\delta = -1.1$, $\Delta x_i = 0.01$ cm, $\Delta t = 0.15$ msec, and the filament defined as the intersection of the $V = 0$ and $\partial_t V = 0$ surfaces. $W(s,t)$ is plotted vs s every 1.25 msec in (a) and 1.5 msec in (b). The arrows in (a) correspond to the times of the four frames in Fig. 1. The insets in (a) and (b) show the trajectories of the wave tip on the top surface (solid line) and bottom surface (dashed line) for the same 200 msec time interval.

[13]. Since the meander path is composed of two outward petals and two elongated arcs of conduction blocks per average period, twistons are created twice per period on average. Twistons can also form in a parameter range where meander would be absent in a 2D sheet because the rotating anisotropy can produce sharp pivot turns around curved sections of elliptical trajectories of the wave tip, and even induce meander [13]. The maximum magnitude of twist along the filament is $\sim 50°/\text{mm}$. This is consistent with the expectation that this magnitude should be $\sim \pi/\ell$, where π is the angle that the wave front rotates during a fast pivot turn around one petal, and $\ell \sim 2$–3 mm is the typical width of a twiston. This width, in turn, is comparable to the thickness of the excitation wave front that is the natural cutoff length scale below which any twist gradient is rapidly smoothed out by diffusion.

Figure 3b is a similar spatiotemporal plot to Fig. 3a, but for the standard FN model. The similarity of the landscapes in Figs. 3a and 3b demonstrates that twistons are a generic feature of vortex dynamics in an excitable medium with a rotating anisotropy, and not unique to the three-variable ionic model studied here. In the FN model, we only observed the weaker turbulence characterized by the transient creation of vortex rings. However, we have not conducted a systematic study of this simpler, but physiologically less relevant, model. Therefore, it cannot be ruled out that a decay similar to Fig. 2 occurs for a higher threshold of wall thickness and/or fiber rotation rate, or different parameters of the model. We have also found that reducing (spatially uniformly) the tissue excitability in the 3V model can suppress the decay into turbulence [13] and that increasing the minimum action potential duration at short cycle length decreases the average number of filaments in the turbulent state.

It may be possible to search for experimental signatures of twistons by measuring the voltage activity on opposite surfaces of the ventricle. The rapid rotation of the wave front on one surface should produce a breakthrough of activation on the opposite surface with a time delay $\sim L/c_{\perp 2}$. This breakthrough, in turn, should consist of a growing target pattern, caused by a curved segment of filament moving towards the surface, followed by the formation of two phase singularities after its collision [13]. Although breakthrough of activations are commonly observed during VF, they have so far remained difficult to interpret. The present results may provide a useful framework to understand their origin.

We thank the American Heart Association for support.

[1] For a review, see Chaos **8**, 1 (1998).
[2] A. T. Winfree, Science **266**, 1003 (1994); in *Computational Biology of the Heart*, edited by A. V. Panfilov and A. V. Holden (John Wiley and Sons Ltd., New York, 1997), p. 101.
[3] R. A. Gray *et al.*, Science **270**, 1222 (1995).
[4] K. M. Kavanagh *et al.*, Circulation **85**, 680 (1992).
[5] M. A. Allessie *et al.*, Eur. Heart J. **10**, 2 (1989).
[6] M. J. Janse *et al.*, in *Cardiac Electrophysiology and Arrhythmias*, edited by D. P. Zipes and J. Jalife (Grune & Stratton, Inc., Orlando, FL, 1985), p. 353.
[7] M. Courtemanche and A. T. Winfree, Int. J. Bifurcation Chaos **1**, 431 (1991); M. Courtemanche, Chaos **6**, 579 (1996).
[8] M. Bär and M. Eiswirth, Phys. Rev. E **48**, R1635 (1993); A. V. Panfilov and P. Hogeweg, Phys. Lett. **176**, 295 (1993); A. Karma, Phys. Rev. Lett. **71**, 1103 (1993); Chaos **4**, 461 (1994); A. Garfinkel *et al.*, J. Clin. Invest. **99**, 1 (1997).
[9] A. V. Panfilov and P. Hogeweg, Phys. Rev. E **53**, 1740 (1996).
[10] V. N. Biktashev *et al.*, Philos. Trans. R. Soc. London A **347**, 611 (1994).
[11] A. V. Panfilov and J. P. Keener, Physica (Amsterdam) **84D**, 545 (1995).
[12] C. Henze, E. Lugosi, and A. T. Winfree, Can. J. Phys. **68**, 683 (1989).
[13] F. Fenton and A. Karma, Chaos **8**, 20 (1998).
[14] G. W. Beeler and H. Reuter, J. Physiol. **268**, 177 (1977).